Bioconjugate Chemistry

Article

pubs.acs.org/bc

Optimizing Protein Coordination to Quantum Dots with Designer Peptidyl Linkers

Kelly Boeneman Gemmill,[†] Jeffrey R Deschamps,[†] James B. Delehanty,[†] Kimihiro Susumu,[‡,§] Michael H. Stewart,[‡] Richard H. Glaven,[†,∥] George P. Anderson,[†] Ellen R. Goldman,[†] Alan L. Huston,[‡] and Igor L. Medintz*[,†]

[†]Center for Bio/Molecular Science and Engineering, Code 6900, and [‡]Optical Sciences Division, Code 5611, U.S. Naval Research Laboratory, Washington, DC 20375, United States

[§]Sotera Defense Solutions, Annapolis Junction, Maryland 20701, United States

[∥]Nova Research Inc., 1900 Elkin Street, Suite 230, Alexandria, Virginia 22308, United States

Supporting Information

ABSTRACT: Semiconductor quantum dots (QDs) demonstrate select optical properties that make them of particular use in biological imaging and biosensing. Controlled attachment of biomolecules such as proteins to the QD surface is thus critically necessary for development of these functional nanobiomaterials. QD surface coatings such as poly(ethylene glycol) impart colloidal stability to the QDs, making them usable in physiological environments, but can impede attachment of proteins due to steric interactions. While this problem is being partially addressed through the development of more compact QD ligands, here we present an alternative and complementary approach to this issue by engineering rigid peptidyl linkers that can be appended onto almost all expressed proteins. The linkers are specifically designed to extend a terminal polyhistidine sequence out from the globular protein structure and penetrate the QD ligand coating to enhance binding by metal-affinity driven coordination. α-Helical linkers of two lengths terminating in either a single or triple hexahistidine motif were fused onto a single-domain antibody; these were then self-assembled onto QDs to create a model immunosensor system targeted against the biothreat agent ricin. We utilized this system to systematically evaluate the peptidyl linker design in functional assays using QDs stabilized with four different types of coating ligands including poly(ethylene glycol). We show that increased linker length, but surprisingly not added histidines, can improve protein to QD attachment and sensor performance despite the surface ligand size with both custom and commercial QD preparations. Implications for these findings on the development of QD-based biosensors are discussed.

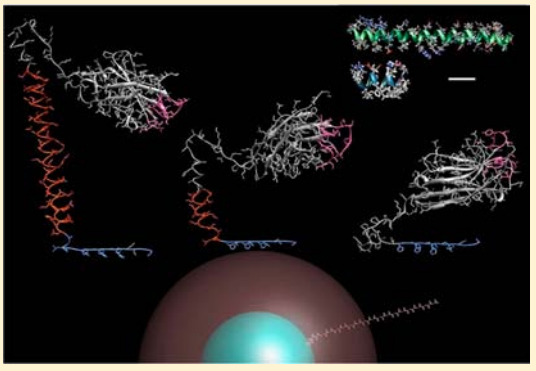

INTRODUCTION

Luminescent semiconductor quantum dots (QDs) have unique photophysical properties that make them ideal probes within many biological applications. They can be custom-synthesized to display unique size-dependent photoluminescence (PL) that are characterized by narrow, Gaussian emissions.[1−4] Their broad excitation profiles increase as a continuum toward the UV portion of the spectrum, allowing for excitation of multiple fluorophores at a single wavelength significantly blue-shifted from their emissions. This allows for concurrent multicolor visualization and provides access to multiplexed assays using a single excitation line. In addition, QDs manifest high quantum yields (QYs) and strong photostability compared to organic dyes or fluorescent proteins. Their high surface to volume ratio allows for the attachment of numerous types of cargo to the surface for a combination of sensing and/or targeting functions. Cumulatively, these features make them potent templates for the assembly of multifunctional nanomaterials with strong potential in clinical diagnostics and drug delivery.[5−8] To date, QDs have also been demonstrated as excellent fluorescence resonance energy transfer (FRET) donors[9,10] and have been used in numerous biological imaging formats including immunohistochemistry, *in situ* hybridization, live cell imaging/biosensing, and even *in vivo* animal labeling.[1−4,11−14]

The continued growth and success of biofunctionalized QDs in these and many other roles remains directly dependent upon control of the conjugation of diverse biomaterials, such as peptides, proteins, drugs, and DNA to the QD surface. For optimal utility, control must be exerted over (1) the number of biomaterials attached per QD, (2) the orientation of the materials on the QD surface, and (3) their binding affinity.[15] Numerous attachment chemistries are currently in use with the two most common being avidin/biotin binding and carbodiimide (EDC)-driven amide bond formation between primary amines on proteins and carboxylated ligands on the QD surface (or the reverse).[16] While useful, these chemistries require purification steps and often result in cross-linking, heterogeneous attachment

Received: December 5, 2012
Revised: January 7, 2013
Published: February 4, 2013

and mixed avidity of the conjugate due to multiple reaction sites on both the QD surface and the protein. Avidin multivalency in conjunction with multiple random biotin placements on the proteins and the large reagent concentrations sometimes required for labeling can result in similar problems.[16−18]

To overcome some of these issues, we have previously demonstrated a noncovalent strategy for conjugation of biomaterials to QDs. It has been shown that proteins, peptides, and even DNA expressing terminal hexahistidine (His_6) sequences can spontaneously self-assemble via metal-affinity-driven coordination to the Zn^{2+} atoms on the surface of CdSe/ZnS core/shell QDs, resulting in stable, biofunctional complexes.[19] This high-affinity interaction, with K_d values in the nanomolar range, allows for rapid self-assembly (mins) and stoichiometric control over valence (ratio of biomolecules per QD) and often results in bioconjugates with structured protein or peptide orientations.[19] Importantly, this bioconjugation strategy also appears to work quite effectively on QDs with varied surface coatings including commercial preparations.[20−22] These attributes have led other groups to start adopting this QD-bioconjugation approach.[1,20,23−25]

One factor that significantly complicates full implementation of this linkage strategy is the physiochemical character of the surface ligands that are used to impart colloidal stability to the inorganic nanocrystals. A wide variety of surface ligands have been developed that improve the solubility of the QDs for biological applications within physiologic conditions.[26,27] Many of these ligands consist of amphiphilic polymer structures and incorporate long poly(ethylene glycol) or PEG repeats to protect the QD surface while providing solubility.[16] While QDs surface-functionalized with such ligands can still allow for self-assembly of His_6-appended peptides or DNA, we have consistently observed that these same surface ligand coatings do not allow for conjugation with larger globular proteins.[18,28] We hypothesize that this is due to steric hindrance constraints and repulsion between the bulky protein structure and the ligand layer of the QD. In contrast, smaller-linear His_6-appended peptides are able to penetrate through and access the QD surface for binding. Although peptides are very versatile, in many cases catalytic, recognition or other biological activities can only be provided by a full protein structure. Therefore, the ability of globular proteins to bind to the surface of soluble QDs in a functional or oriented manner remains critically important to the future capabilities of QD-based bionanostructures.

While this issue is being partially addressed by the development of more compact surfaces and more complex ligands that display requisite binding groups,[1,16,21] here, we present an alternate, complementary route by engineering peptidyl linkers which allow for penetration through the bulk QD surface ligand layers. For these purposes, we choose to use α-helical linkers for their well-understood structural characteristics and rigidity. We first characterize the persistence length and QD orientation of two α-helical peptidyl linkers using FRET measurements (Figure 1). For functional analysis, the peptides are appended onto an anti-ricin single-domain antibody (SdAb) fragment which, when self-assembled to QDs, provides an immunoreagent for the detection of the biothreat agent ricin in direct immunoassay formats. Using this model system, we found that the assembly and functionality of the QD-conjugated immunosensor is dependent upon the linker length, indicating increased ability of the sdAb to overcome steric hindrance by penetrating the ligand layers and bind to the QD surface. This result remained consistent during testing of QDs prepared with four different types of surface ligands: (1) dihydrolipoic acid (DHLA), (2) DHLA-PEG, (3) DHLA-compact-ligand 4 (CL4), and (4) a commercial amphiphilic polymer (Invitrogen Qdot ITK QDs); see Scheme 1 for structures.[21] We also evaluate whether increasing the number of terminal QD-coordinating His_6-motifs from one to three can help improve assembly of both the original and linker-appended derivative proteins to the QDs. The results are discussed in the context of developing improved QD−protein bioconjugates.

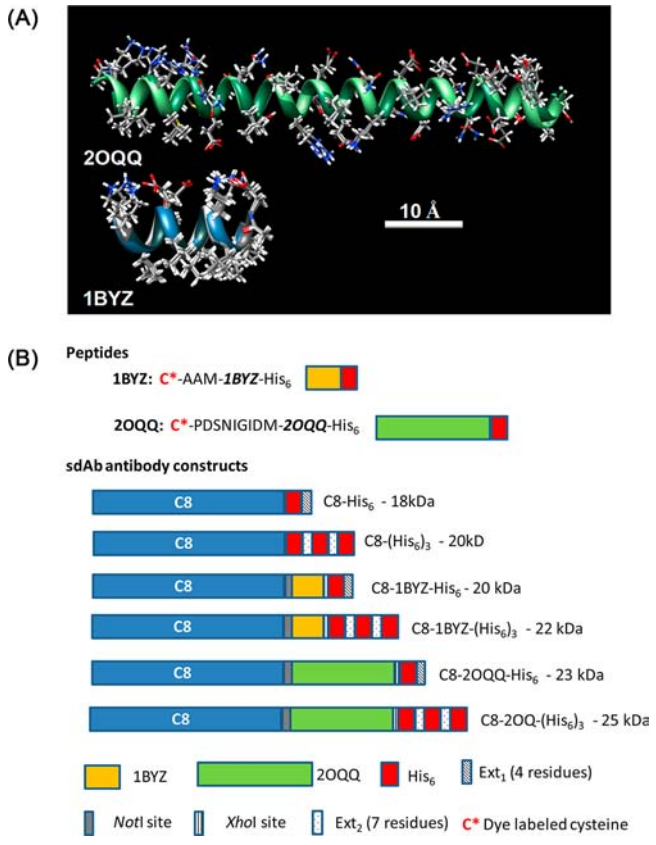

Figure 1. (A) Structures of the 1BYZ and 2OQQ α-helical linkers derived from their crystallographic coordinates. The helices are highlighted as a ribbon with side chain chemical functionalities shown. For 1BYZ, the nonpolar region is on the lower portion of the helix and the polar region on the upper portion. (B) Schematic of the 1BYZ and 2OQQ peptides and C8 single-domain antibody constructs used in this study. The top peptide structures represent the constructs use for QD-FRET experiments, while the bottom sdAb constructs were used in immunoassays.

MATERIALS AND METHODS

Peptide and Protein Cloning. *1BYZ.* Complementary overlapping oligos 5′-GCGGCGTGCGAACTGCTGAAAAAACTGCTGGAAGAACTGAAAGGCCACCACCACCACCACCACCAGATG-3′ and 5′-CTGGTGGTGGTGGTGGTGGTGGCCTTTCAGTTCTTCCAGCAGTTTTTTCAGCAGTTCGCACGCCGCCAT-3′ (Eurofins EWG Operon) were annealed and ligated to create concatamers of the His_6-labeled 1BYZ coding sequences. PCR primers 5′-GCTATAACAGATGCTGGCGGCGTGC-3′ and 5′-GCATATTCAGCATCTGGTGGTGGTGGTG-3′ were used to amplify the repeats and add *AlwN*1 restriction sites (underlined) to both the 3′- and 5′-ends. PCR products were purified, digested with *AlwN*1 (New England Biolabs), and ligated into an *AlwN*1- and calf intestinal alkaline phosphatase- (CIP) (New England Biolabs) treated pET31b vector (Novagen) as an in-frame fusion with

dx.doi.org/10.1021/bc300644p | *Bioconjugate Chem.* 2013, 24, 269−281

Scheme 1. Chemical Structures of the DHLA, DHLA-PEG-OMe, CL4, and Amphiphilic Carboxylated ITK Polymer QD Ligands Used in This Study

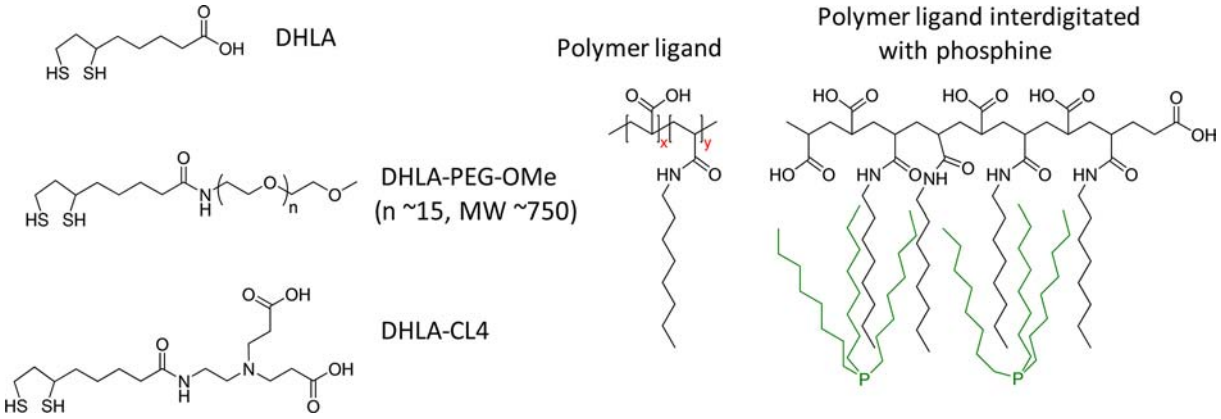

the ketosteroid isomerase (KSI) protein. Final constructs were confirmed via restriction digest analysis and DNA sequencing and contained two 1BYZ coding sequences.

2OQQ. Complementary oligos with bacterial codons optimized for 2OQQ expression and a 5′-cysteine for peptide labeling, a 3′-His_6 tag, and overhanging 5′ and 3′ *BamH*I restriction sites (underlined) 5′-GGATCCTGCGGCAGCGCGTATCTGAGCGAACTG-GAAAACCGCGTGAAAGATCTGGAAAACAAAAACAGCG-AACTGGAAGAACGCCTGAGCACCCTGCAAACGAAAAC-CAGATGCTGCGCCATATTCTGAAAAACCACCACCACC-ACCACCACTGA-3′ and 5′-GGATCCTCAGTGGTGGTGGT-GGTGGTGGTTTTTCAGAATATGGCGCAGCATCTGGTTT-TCGTTCTGCAGGGTGCTCAGGCGTTCTTCCAGT-TCGCTGTTTTTGTTTTCCAGATCTTTCACGCGGTTTT-CCAGTTCGCTCAGATACGCGCTGCCGCA-3′ (Eurofins EWG Operon) were annealed and ligated into a T-vector (Promega). The oligo was then digested out of the T-vector with B*amH*1 and ligated into a *BamH*1 digested, CIP-treated pET22b vector (Novagen). The final construct was confirmed by restriction digestion and DNA sequencing.

C8 sdAb. The C8 single domain anti-ricin antibody[29] was subcloned into a pET22b expression vector (Novagen) between the *Nco*1 and *Not*1 sites and the modified 1BYZ and 2OQQ sequences described above were inserted between *Not*1 and *Xho*1 after the C8 coding sequence and before the His_6 tag (Genscript, Inc.). Each linker was inserted into vectors with either a single His_6 tag or three His_6 tags, $(His_6)_3$, separated by a seven-residue extension (AGSAGVE) (Figure 1B). Constructs were confirmed by restriction digest analysis and DNA sequencing.

Peptide Expression, Purification, and Labeling. *1BYZ Peptide.* The peptide was produced as a fusion with KSI protein, an insoluble protein carrier expressed from an inducible promoter sequence. A pET31b vector (Novagen) containing KSI fused tandem 1BYZ coding sequences described above was transformed into BL21(DE3)pLysS cells (Promega) and grown in 200 mL of Luria broth (LB) with 50 μg/mL carbenicillin and 34 μg/mL chloramphenicol overnight at 37 °C. Cultures were diluted into 1.2 L of LB with above antibiotics and grown for 3 h at 37 °C before a 3 h induction with 1 mM isopropyl β-D-1-thiogalactopyranoside (IPTG). The culture was centrifuged for 10 min at 12 000*g* and resuspended in 120 mL binding buffer (5 mM imidazole, 40 mM Tris HCl pH 7.9, 500 mM NaCl). Thirty milliliters of cell suspension was lysed at a time by sonicating 7 times for 1 min on ice. Sonicates were centrifuged, washed with 30 mL of binding buffer, and then centrifuged again. Resuspension and centrifugation in 30 mL binding buffer with 6 M guanidine HCl allowed for solubilization of the KSI-IBYZ tandem fusion in the supernatant and pelleting of cell debris. Purification was performed using a His-bind buffer kit (Novagen) with the addition of 6 M guanidine HCl to the buffers to maintain fusion protein solubility. Elution was performed with 15 mL of binding buffer supplemented with 6 M guanidine HCl and 300 mM imidazole. Protein elution was visibly apparent by the brownish color of eluate and detected by SDS-PAGE electrophoresis (Supporting Information). Eluted protein was dialyzed twice against 4 L of ddH20 to remove imidazole and guanidine HCl. Precipitated protein was retrieved, pelleted, and frozen at −20 °C for storage and later cleavage.

For cleavage of individual IBYZ peptides from the insoluble KSI protein, fusion pellets from approximately 200 mL of the original cell culture were resuspended with stirring in 6 mL 80% formic acid in a round-bottom flask with 0.2 g cyanogen bromide and nitrogen bubbling overnight. Note that formic acid and cyanogen bromide are both highly toxic and must be handled with appropriate care. The suspension was dried in a rotary evaporator and resuspended in 20 mM potassium phosphate with 100 mM NaCl, pH 7.4. The insoluble KSI protein was removed by centrifugation, and the soluble 1BYZ single peptides were then further purified with nickel(II)-nitrilotriacetic acid (Ni^{2+}-NTA)-agarose (Qiagen) and desalted using a reverse-phase oligonucleotide purification cartridge (OPC, Applied Biosystems) with triethylamine acetate (TEAA) buffer. The purified peptide was quantitated by UV−visible absorption, aliquoted, dried *in vacuo*, and stored at −20 °C.[30]

2OQQ Peptide. 2OQQ was expressed in the pET22b vector (Novagen), which contains a pelB leader sequence that directs the peptide to the periplasmic space and a signal peptidase site for leader sequence removal. The expression vector was transformed into BL21(DE3) cells and the protein purified by periplasmic purification.[14,29] Two hundred milliliters of overnight culture was diluted into 1 L of LB supplemented with 100 ug/mL carbenicillin and grown for 3 h at 37 °C with shaking. Cells were then induced with 1 mM IPTG for 5 h. Cells were harvested by centrifugation and resuspended in 100 mL 0.1 M Tris pH 7.5/0.75 M sucrose buffer and evenly divided. Osmotic shock was achieved by the addition of 40 mL of 1 mM EDTA slowly added dropwise to each bottle while gently shaking, followed by 2 mL 0.5 M $MgCl_2$. Lysate was centrifuged at 7000*g* for 10 min twice to remove cell debris. The supernatant was added to 10 mL of 50% Ni-NTA slurry

dx.doi.org/10.1021/bc300644p | *Bioconjugate Chem.* 2013, 24, 269−281

pre-equilibrated with 0.1 M Tris pH 7.5/0.75 M sucrose and incubated overnight with shaking at 4 °C. The Ni-NTA column was then washed with phosphate buffered saline (PBS, 10 mM phosphate, 0.137 M NaCl, 0.3 mM KCl, pH 7.4) and peptide was eluted using PBS supplemented with 300 mM imidazole. Peptide containing fractions were dialyzed twice overnight in 4 L PBS.

Peptide–Dye Labeling. Both 1BYZ and 2OQQ peptides in PBS were reduced using Cleland's reductacryl reagent (EMD Millipore) and labeled with agitation overnight using at least a 2-fold excess of Cy3 maleimide (Amersham Biosciences).[30] Dye-labeled peptide was purified with Ni^{2+}-NTA-agarose and desalted using an OPC with TEAA buffer. The purified, labeled peptide was quantitated by UV–vis absorption, aliquoted, dried *in vacuo*, and stored at −20 °C until needed.[30]

C8 sdAb Purification. The expression vectors for the C8 sdAbs, both with and without 1BYZ and 2OQQ linkers and with His_6 and $(His_6)_3$ tags (Figure 1), were transformed into an *E. coli* Rosetta2(DE3)pLysS strain (Novagen) for protein production. Extensions 1 and 2 were residues added in during the peptide cloning process. SdAb proteins were isolated from the periplasmic compartment as described above and purified using immobilized metal affinity chromatography (IMAC) with Nickel-sepharose resin (GE-Healthcare). Protein was eluted with 300 mM imidazole and fractions were identified by the UV absorption at 280 nm, pooled, and further purified via Fast protein liquid chromatography (FPLC) using a Superdex 75 10/300 GL column and Akta FPLC system (GE Healthcare). Purification was confirmed via SDS-PAGE analysis of proteins. SDS-PAGE also confirmed size differences due to insertion of the helical linkers (Supporting Information).

Quantum Dots. 525 and 530 nm emitting CdSe/ZnS core/shell QDs were synthesized from organometallic precursors as previously described.[21] The native organic-functionalized QDs underwent cap exchange with dihydrolipoic acid (DHLA), poly(ethylene glycol)-appended DHLA terminating in a neutral methoxy group (DHLA-PEG-OMe, PEG average molecular weight ∼750), or CL4 compact zwitterionic ligands as described previously.[21,26] Note that the terms DHLA-PEG-OMe and DHLA-PEG are used interchangeably here, as are CL4 and DHLA-CL4 and designate the same materials. 605 nm emitting carboxyl ITK QDs were purchased from Life Technologies. See Scheme 1 for surface ligand structures.

QD–Peptide FRET and FRET Analysis. Fifteen picomoles of DHLA-PEG QDs per reaction were self-assembled to the indicated numbers of peptides per QD in 1× PBS. Steady-state ensemble fluorescence spectra were collected from solutions of QD-labeled peptide bioconjugates with a Tecan Safire Dual Monochromator Multifunction Microtiter Plate Reader (Tecan, Research Triangle Park, NC) using 300 nm excitation. For energy transfer efficiency analysis, the direct excitation contribution to the emission from each acceptor (determined from control solutions) was subtracted from the measured spectra and the resulting composite spectra were deconvoluted to identify the contributions from the QD emission and the sensitized component of Cy3, similar to the methods described previously.[10] For each QD–dye donor–acceptor pair, the Förster distance (R_0) corresponding to a donor–acceptor separation resulting in 50% energy transfer efficiency was calculated using the expression[31]

$$R_0 = 9.78 \times 10^3 [K^2 \acute{n}^{-4} Q_D J(\lambda)]^{1/6} \quad (1)$$

where $\acute{n}$ is the refractive index of the medium, Q_D is the QY of the donor, $J(\lambda)$ is the spectral overlap integral, and κ^2 is the dipole orientation factor. R_0 is typically given in units of in Å or nm, while $J(\lambda)$ is in units of $cm^3\ M^{-1}$. We use a κ^2 of 2/3 which is appropriate for the random dipole orientations arising within these self-assembled configurations.[10,32,33] The average energy transfer efficiency E was extracted for each set of QDs and dye-labeled peptide using the equation

$$E = (F_D - F_{DA})/F_D \quad (2)$$

where F_D and F_{DA} are the fluorescence intensities of the donor alone and donor in the presence of acceptor(s), respectively.[31] The polyhistidine-driven self-assembly of dye-labeled peptide to QD yields a central nanocrystal conjugated to a quasi centrosymmetric distribution of acceptors characterized by consistent average center-to-center separation distances (r).[32] When analyzed using Förster dipole–dipole formalism, the energy transfer efficiency data can be fit to the expression[32]

$$E = \frac{nR_0^6}{nR_0^6 + r^6} \quad (3)$$

where n is the average number of acceptors per QD. For conjugates that are self-assembled with relatively low numbers of acceptors (<4), heterogeneity in conjugate valence can be probed and accounted for by using a Poisson distribution function, $p(N, n)$, during the fitting of the efficiency data[33]

$$E = \sum_n p(N, n)E(n) \quad \text{and} \quad p(N, n) = N^n \frac{e^{-N}}{n!} \quad (4)$$

where n designates the exact numbers of acceptors (valence) for conjugates with a nominal average valence of N.

Immunoassays. High-binding 96 microwell plates (Nunc, Thermo Scientific) were coated with the indicated concentrations of ricin antigen (Vector) in PBS at 4 °C overnight. The plates were blocked with 4% nonfat powdered milk (Carnation) in PBS at room temperature for 1–2 h, then washed 5 times with PBS. Optimal QD concentrations for each sample were determined empirically and varied due to the differences in QY. Twenty-five nanomolar DHLA-based QDs was used, while 5 nM of the brighter CL4 and ITK QDs were used. The indicated numbers of C8 sdAb proteins were self-assembled to the QDs at room temperature for 30 min in PBS (except DHLA-QD reactions which were performed in 10 mM sodium tetraborate buffer pH 8.5). This molar addition of protein per QD forms the basis of the ratios of $protein_n$/QD indicated throughout the following. Self-assembly reactions with ITK QDs included 10 μM $NiCl_2$ (Sigma-Aldrich) to help chelate the His_6 on the QD surface.[23,34] DHLA-PEG, CL4, and ITK QD conjugates were filtered through 50 000 MW spin filters (Millipore) to remove excess sdAbs and recalibrated for QD loss by measurement of QD PL. The QD–peptide conjugates were then added to the washed plates and incubated for 90 min. Plates were washed with 1× PBS and refilled with 1× PBS prior to analysis. DHLA–QD conjugates were added to the plates without the filtration step due to precipitation issues, and washing and readings were done in borate buffer. In the event of high background binding in the absence of ricin, a second wash with PBS or borate supplemented with 0.05% Tween 20 was added. Background QD binding was subtracted in the normalized data.

Structural Simulations. *SdAb.* A search was conducted in the protein database (PDB, www.rcsb.org) using the sequence of the C8 sdAb and the FASTA algorithm. Only structures

Table 1. Peptides, sdAb, and Polyhistidine Sequences Used in This Study[a]

name	sequence	helix length (Å)	M_w	PI/Charge pH 7.4 (8.5)	ref
1BYZ	ELL**KKLLEE**LKG	11.3	1413	7.1/−0.2 (−0.9)	www.rcsb.org[36]
2OQQ	GSAY**LSELENRVK**DLENKNS-**ELEERLS**TLQN**ENQMLRHI**LKN	57.5	4958	4.9/−2.1 (−0.9)	www.rcsb.org[37]
C8 anti-Ricin sdAb	MAEVQLQASGGGLVQGGDSLRLSCAASGRTLGDYGVAWFR-QAPGKEREFVSVISRSTIITDYANSVKGRFTISRDNAK-NAVYLQMNSLKPEDTAVYYCAVIANPVYATSRNSDDY-GHWGQGTQVTVSSEPKTPKPQPAASGAEFAAALE	Dimensions: L × W × H 40 × 30 × 25	15871	6.9/−0.3 (−2.1)	29
His_6	HHHHHH	–	840	8.4/0.3 (0)	This study
$(His_6)_3$	HHHHHHAGSAGVEHHHHHHAGSAGVEHHHHHH	–	3630	7.0/−0.9 (−1.7)	This study

[a]Bold and underlined = helical regions predicted by nnpredict (Donald Kneller (1991) Regents of the University of California, http://www.cmpharm.ucsf.edu/nomi/nnpredict.html).

determined by X-ray crystallography were considered to eliminate the multiple conformations normally associated with NMR structures. Additionally, structures from llama proteins were given a higher weight as the origin of the C8 sdAb was a llama. Of the 2453 hits identified, PDB entry 3R0M was one of the two highest ranked overall, before applying additional criteria. The other top hit (3RJQ) was an antibody in complex with its antigen and had a lower resolution (2.60 Å vs 1.50 Å). Entry 3R0M with a score of 113 was used as the starting point for modeling (Figure S5). It should be noted that no structural information was available for the sequence highlighted in blue in 3R0M (Figure S5). A second search was conducted with the sequence EPKTPKPQPAASGAE-FAAALE (AAALE is from the cloning vector and codes for the *Not*1 and *Xho*1 sites while EPKTPKPQP is from the upper hinge region) using the FASTA algorithm. This resulted in only three hits: 3I4J—used in the modeling, 3V0A—no structural information for target sequence, and 2DBA—an NMR structure. The lack of structural information for this sequence in the original query, in combination with one of the hits in this additional search, and the fact that this sequence is present in a disordered portion of the NMR structure (Figure S6) suggests that the conformation of this region is likely to be highly variable. Despite this variability, the NMR and X-ray structures agree on a helical conformation for the remaining C-terminus of this peptide.

Single-Domain Antibody Model with Linker and QD Binding Domain. The model of the sdAb with the selected linkers and QD binding domain (Figure 5) can be thought of as consisting of three components: the sdAb, the linker (a helical peptide used to increase the separation between the sdAb and QD), and a histidine-rich tail used to assemble the construct to a QD. Each component is modeled separately and then assembled into the final sdAb model. In this manner, the effect of different spacers (or no spacer) can be investigated. The final sdAb model was constructed using the coordinates from 3R0M, modified as described and linked to the structure of the C-terminal region extracted from 3V0A. After merging, the resulting model protein was energy minimized using the tools in *Chimera 1.4.1*.[35] The model sdAb was the starting point for the three models shown in Figure 5: the model sdAb with no linker on the C-terminus (right), the model sdAb with a short 1BYZ helical linker (center), and the model with a long 2OQQ helical linker (left). For comparison, a QD (5.6 nm diameter) with a PEG-750 coating is shown at the bottom of the figure. It should be noted that the PEG-750 coating creates a shell only 2.9 nm thick, much less than fully extended PEG-750.[21] Further information on the modeling can be found in the Supporting Information.

RESULTS

Peptide Design and Expression. Initial work focused on designing two peptidyl linker sequences of differing lengths. As these linkers had to incorporate rigidity within their sequence, helical motifs were among the primary search criteria. A number of putative helical linkers were identified from the PDB and two helices were chosen; see Table 1. 1BYZ is an amphiphilic 12-residue peptide that was designed *de novo* to form an α-helix where the apolar leucine side chains would extend from one side, and the charged lysine and glutamate side chains are displayed on the other face. This amphiphilic character then drives the self-association of an antiparallel α-helical bundle, which was subsequently confirmed by crystallographic analysis.[36] The crystal structure of this short peptide contains four independent molecules with unique conformations of the side chains. The predicted end-to-end or persistence length of this helical structure is ∼11.3 Å (Figure 1A). The second peptidyl sequence selected was 2OQQ and originates from a leucine zipper domain in the *Arabidopsis thaliana* HY5 transcription factor.[37] This 42-residue peptide is predicted to assume an extended ∼57.5 Å structure that is dominated by a helix (see Figure 1A). The crystal structure of 2OQQ contains two independent molecules with unique conformations of the side chains and slightly different conformations of the helices. This peptide has identifiable polar and nonpolar domains but does not have such a dramatic segregation of these domains as found in 1BYZ.

Unique N-terminal cysteines for further dye-labeling and C-terminal His_6 tags were engineered onto each peptide. Some additional N-terminal residues were added to each peptide during the cloning process (Figure 1B). Both peptides were expressed and purified in *E. coli* as described in detail in the Methods. As short peptides are often toxic to bacterial cells, 1BYZ was expressed as a concatamer fused to the insoluble ketosteroid isomerase protein (KSI). Cyanogen bromide cleavage released the soluble 1BYZ from the insoluble carrier protein after extraction from the cells.[38] 2OQQ was expressed and purified by standard periplasmic purification methods.[29] Both peptides were purified by Ni-NTA columns, labeled with Cy3-maleimide and quantified using the Cy3 absorbance (150 000 M^{-1} cm^{-1} ∼550 nm) as described.[30]

Estimation of Peptide Rigidity by FRET. First, we evaluated the orientation and extension the peptides assume as they self-assemble to the surface of the PEGylated QDs by

dx.doi.org/10.1021/bc300644p | *Bioconjugate Chem.* 2013, 24, 269−281

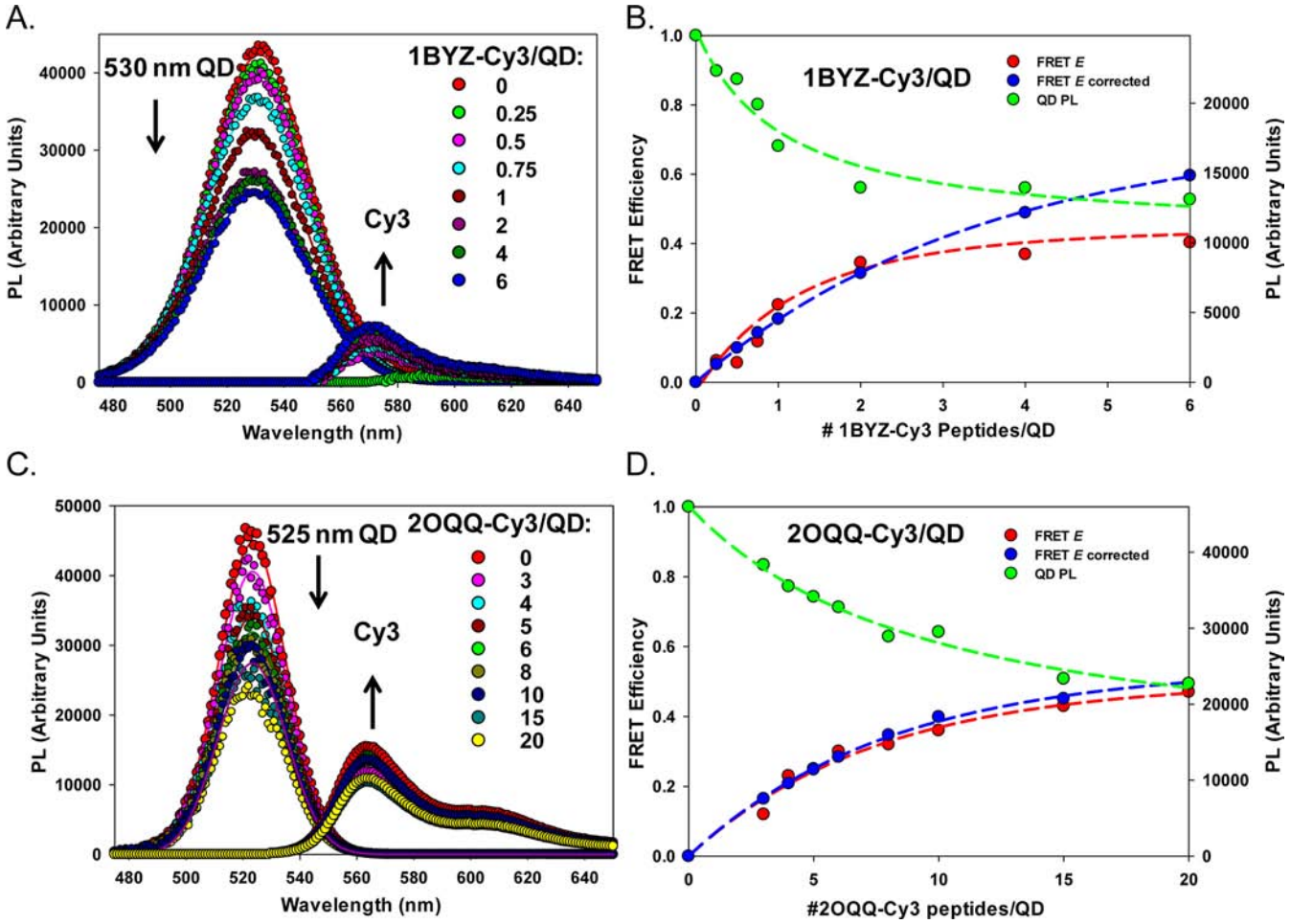

Figure 2. (A) Deconvoluted and background-corrected FRET spectra for 530 nm emitting DHLA-PEG QDs assembled with the indicated ratios of Cy3-labeled 1BYZ. (B) Respective plots of QD PL loss, FRET *E*, and FRET *E* corrected versus the indicated ratio of acceptor label for the data in panel A. (C) Deconvoluted and background-corrected FRET spectra for 525 nm emitting DHLA-PEG QDs assembled with the indicated ratios of Cy3-labeled 2OQQ. (D) Respective plots of QD PL loss, FRET *E*, and FRET *E* corrected versus the indicated ratio of acceptor label for the data in panel C.

His_6-driven metal affinity coordination. This serves to confirm that the peptide's termini penetrated the PEG layer and assumed an orientation with the helical portion extending directly out from the QD surface as designed. The PEGylated type of QD was chosen for this, as it is the most problematic for protein assembly. Deconvoluted spectra of FRET between 530 and 525 nm DHLA-PEG-coated QD donors assembled with the indicated increasing ratio of Cy3-acceptor labeled 1BYZ and 2OQQ, respectively, are shown in Figure 2A,C. Loss of the QD donor PL is clearly observed following assembly with increased amounts of labeled-peptide and this is concurrent with an increase in sensitized Cy3 fluorescence. The corresponding QD donor PL loss, FRET efficiency *E*, and Poisson-corrected FRET *E* were determined as described in the Methods and are shown in Figure 2B,D. For both QD assemblies, FRET *E* peaks at comparable levels of 40−50%; however, conjugates formed with 1BYZ reach this level at a much lower valence (~4 peptides/QD) than conjugates formed with 2OQQ (~20 peptides/QD). This result strongly correlates to the shorter size of the 1BYZ peptide which should yield a higher FRET *E* at lower valences due to the acceptor dyes proximity to the QD surface. In contrast, the larger 2OQQ peptide should quench QD PL at a slower rate which was also seen. The concordance between FRET *E* and the corrected values at low valency confirms that there was minimal heterogeneity during peptide self-assembly to the QDs.

Predictions of QD donor to dye acceptor center-to-center separation distances *r* were made by considering the diameter of the QD, peptide length and rigidity, dye size, and attachment linker structure along with predicted peptide binding orientation.[18] Experimental *r* values were then calculated from the FRET data presented in Figure 2 using eqs 3 and 4. Comparison of these values in Table 2 reveals that the measured 1BYZ peptide length appears to be slightly longer than predicted, 6.5 vs 5.5 nm (+18% difference), while the

Table 2. FRET Distances Determined in This Study

donor QDs	quantum yield	Cy3-labeled peptide acceptor	expected r^a	experimental r^b
530 nm DHLA-PEG	0.2	1BYZ	5.5 nm	6.5 nm
525 nm DHLA-PEG	0.2	2OQQ	10 nm	8.9 nm

[a]Expected *r* corresponds to the estimated QD center to Cy3 center separation distance as described in the text. [b]Experimental *r* corresponds to the QD center to Cy3 center separation distance determined from FRET analysis.

dx.doi.org/10.1021/bc300644p | *Bioconjugate Chem.* 2013, 24, 269−281

2OQQ construct is slightly shorter than predicted 8.9 vs 10 nm (−11% difference). These deviations may be partially due to the range of rotational motion the peptides can assume once attached to the QD surface, as has been shown for similar His_6-peptido-DNA constructs assembled on PEGylated QDs.[18,39] It is also important to note that these experimental values were within 10−20% of the predicted values, which is at or near the calculation error rate normally encountered in similar QD FRET constructs.[18,39] Given these results, we conclude that our α-helical linkers are of predicted size and form a rigid helix that can penetrate the PEG layer, coordinate to the QD surface, while still allowing for extension away from the QD surface and out of the DHLA-PEG layer.

Antibody Constructs and the Different QD Samples. SdAbs are the recombinantly expressed variable domain derived from the heavy chain only antibodies found in camelids. Although they bind antigen through a single variable domain, they have comparable antigen affinity to standard antibodies and in addition possess structural characteristics that make them ideal for many biosensing purposes, including conjugation with nanomaterials.[14] They are generally small and compact (~16 kDa), demonstrate elevated temperature stability, and may be able to recognize epitopes nonaccessible to conventional antibodies.[29,40] The C8 sdAb utilized here has previously demonstrated high affinity toward the biothreat agent ricin, a naturally derived, highly toxic protein from the castor oil plant *Ricinus communis*. This sdAb is readily expressed and purified from *E. coli*;[29,41] however, the C8 sdAb is still large enough that it will not directly assemble onto PEGylated QDs (data not shown). As such, we chose to use it as a model protein within these studies.

We engineered our two helical linkers into the open reading frame of the antibody fragment between the sdAb coding sequence and the His_6 tag. We further added the linkers into vectors with both a single and a $(His_6)_3$ tag to test if the presence of extra histidines may contribute to improving QD surface binding/coordination capabilities. The single and triple His_6-parent C8 SdAbs along with constructs expressing both the peptide linkers were expressed and purified as described in the Methods. Schematics of the fragment constructs are illustrated in Figure 1B. Extension 1 and 2 were residues added in during the peptide cloning process. Expression and purification was confirmed by a single band of the expected size using SDS-PAGE analysis (Supporting Information).

For this portion of the study, QDs prepared and made soluble with the four different surface ligands were initially tested for bioconjugate assembly and functionality against each of the above-described sdAb variants. We examined DHLA-PEG, DHLA, and compact ligand CL4-coated QDs[21] to evaluate how ligand composition and size can affect protein assembly to QDs. DHLA ligands utilize the charged carboxyl groups to impart colloidal stability to the QDs and necessitate slightly basic buffer to maintain the deprotonated state. The ethylene oxide repeat of the PEG and the zwitterionic nature of the CL4 ligand both mediate solubility in a relatively pH insensitive manner.[21] Beyond our in-house materials, commercially available ITK Qdots prepared with a carboxylated polymer surface were also tested. *A priori*, the histidine tag of the single domain antibodies are unlikely to penetrate this ligand layer and access the QD surface itself as the polymer encapsulates the native organic ligand still present on the QD surface (Scheme 1). However, in the presence of a small amount of added Ni^{2+}, it has been shown that polyhistidine appended proteins are able to bind to the carboxylated ends of the ligands via a chelation process similar to that of Ni-NTA during protein purification.[23,24,34] Experiments with these QDs would thus offer information on the activity of the helical linkers within the context of a slightly modified method of protein/QD surface conjugation.

Immunoassay Results. *Linker Effects.* The above purified C8 sdAbs, with and without the linkers and expressing single or $(His_6)_3$ tags, were self-assembled to QDs with the different surface ligand coatings and used in preliminary direct binding immunoassays to detect ricin antigen. This functional test was designed to verify that the conjugate was indeed formed and remained intact through all of the assay wash and binding steps. We chose an average of five proteins per QD as our nominal initial assembly valency as this represents less than maximal surface binding and should not induce any steric effects on the binding. All samples were tested on wells where 5 μg/mL ricin had been used for coating. As shown in Figure 3A which compared results from the His_6-constructs, in the absence of linker ("No Linker" sample), there is a limited ability of the DHLA-PEG QD-sdAb bioconjugates to bind the antigen target. This is consistent with previous results where globular protein binding to the surface of DHLA-PEG QDs was shown to be sterically hindered.[28] In contrast, assembly and binding were clearly improved with the addition of the 1BYZ linker and significantly more so with the longer 2OQQ linker. Assembly and binding also improved to QDs prepared with more compact ligands such as CL4, where the steric hindrance of the surface coating should be much lower. Qdot ITK carboxyl QDs were expected to bind protein at the carboxylated ends of their surface ligands by interaction with Ni^{2+}. We confirmed that, in the absence of nickel, binding was minimal (Supporting Information). This also confirmed that the His_6 tags are not penetrating through the surface ligand layer, and are likely being chelated by the coordinated Ni^{2+}. Unconjugated control QDs processed in the same manner showed no effective ricin binding capacity. Assays with the DHLA-coated QDs also consistently showed the poorest performance, a result we attribute to a combination of the charged nature of this ligand coating in conjunction with use of a higher pH buffer which is needed to keep these QDs colloidally stable. We also confirmed that in the absence of QDs the binding abilities of the C8-His_6, C8-1BYZ-His_6, and C8-2OQQ-His_6 constructs to ricin were all comparable via surface plasmon resonance (SPR) analysis (Supporting Information).[41,42]

Figure 3B shows comparable data from experiments conducted with the $(His_6)_3$ tag products. Addition of multiple His_6 tags has been shown to improve histidine-dependent binding in QD assemblies and other applications such as Ni-NTA column purifications.[14,19,43] We found that, while the $(His_6)_3$ tags did allow for construct assembly and antigen binding, overall binding capacity was not increased, and in many cases was paradoxically decreased, compared to the comparable single His_6 tag construct. A dependence of binding ability on linker length was also not observed in these variants either. Several factors may contribute to these rather unexpected results. There are reports in the literature that some His_6-tags can be unstable and prone to degradation.[44] We also postulate that the triple tag may introduce a high level of flexibility into the terminus, not allowing the rigid linkers to act as needed to extend the sdAb away from the QD surface (Supporting Information). The CL4 QDs did, however, manifest significantly more binding to target than the other

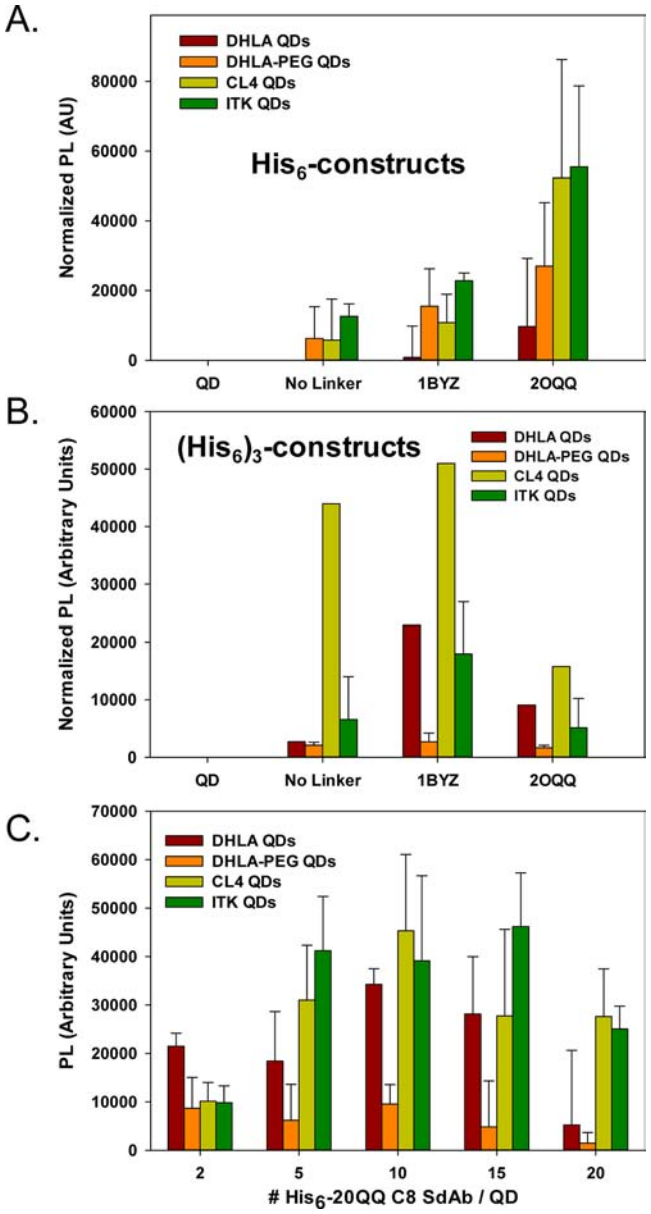

Figure 3. Comparative immunoassay data for four types of QD-C8 sdAb conjugates assayed against 5 μg/mL ricin. An average of 5 proteins/QD was used. (A) Data for the His_6-constructs versus unconjugated control QDs. (B) Data for the $(His_6)_3$-constructs versus unconjugated control QDs. (C) Titration of increasing C8−2OQQ-His_6 sdAb ratio against 5 μg/mL ricin for the four different QD materials.

QD preparations which suggests that this may not be a degradation issue, but rather one of accessing the surface for effective coordination. The zwitterionic nature of the CL4 ligands may also interact with the $(His_6)_3$ constructs in an unknown manner which could promote coordination. The exact nature and structure of how the individual adjacent His residues in the His_6-tag coordinate to atoms on the QD surface while maneuvering between the assembled ligand moieties still remains unknown. Overall, we found the single His_6-tag to be more predictable and thus used them for the remainder of this study.

Valency Effects. In Figure 3C, we titrated the most effective construct, the C8-2OQQ-His_6 sdAb, onto all 4 QD materials in an attempt to determine the optimum valence or QD assembly ratio. Previous modeling analysis estimated that approximately 30 myoglobin proteins, that are very comparable in size to the C8 (~17 kDa vs ~16 kDa, respectively) should be able to bind to the DHLA-based QDs.[45] We utilize ref 45 as the basis for estimating the maximum number of similar-sized proteins that should bind to the DHLA-based QDs (≤30) and we base our assemblies on this. We observed an increase in the efficiency of the immunosensor up to about an average ratio of ten proteins per QD. We began to see a decrease in antigen binding activity above a valence of 10 for DHLA, DHLA-PEG, and CL4 QDs and above 15 for ITK QDs (Figure 3C). The slightly larger value for the ITK QDs is believed to arise from its much larger surface area and hydrodynamic radius.[46] The specific cause of the decrease in binding activity is unknown, but may be related to specific structural characteristics of the C8 sdAb and steric interactions on the QD surface after assembly. Indeed, the asymmetric or wedge structure of myoglobin did affect its packing orientation when self-assembled to QDs in the same manner.[45] A ratio of 5 was thus chosen as an optimal working valence for further experiments, as it is below the activity saturation level for all QDs while still showing acceptable antigen binding capacity.

Comparison of Ricin Binding Sensitivity among the Four QD Immunosensors. Last, each of the four QD materials were assembled with an average of five C8-2OQQ-His_6 sdAbs and tested against ricin using the immunoassay format to determine and compare the dynamic sensing ranges (DSR_{app}),[47] limits of detection (LOD_{app}), and binding affinity (K_{dapp}). It is important to point out that these are only apparent values we estimate and use to compare the activity among the QD materials. Although the microtiter plates are exposed to a fixed series of ricin concentrations, their binding capacity determines the actual amount of ricin present which will saturate at concentrations below the maximum. We thus stipulate that these values are just comparative estimates, as the focus here is more on comparison among QD conjugates as a function of coating chemistry.

Figure 4 and Table 3 present results from these experiments where QD-immunosensing conjugates were assayed against the indicated concentration range of ricin. The estimated K_{dapp} values extracted from our data ranged from 0.14 to 0.32 nM and indicate that the C8 sdAb is essentially unchanged by the insertion of the 2OQQ terminal linker and continues to function in essentially the same kinetic manner. The proteins performed similarly when immobilized for SPR analysis of ricin binding (see Supporting Information). In contrast to this general concordance, the range of values estimated for the limits of detection (LOD_{app}) varied quite widely from 50 up to 8700 ng/mL for the CL4 and DHLA QDs, respectively. The dynamic sensing ranges (DSR_{app} ~10−90% PL change for each construct) were also quite broad, although the range among the lower (850−1700 ng/mL) and higher values (68 500−137 000 ng/mL) across all four QDs are within 2-fold of each other. Interestingly, although we only treat the K_{dapp} as an apparent estimate, our values appear to be comparable to the previously published K_d for the same C8 of 0.35 nM.[41] In contrast, our LOD_{app} values are not as sensitive as the 1.6 ng/mL LOD reported for a sandwich immunoassay format in ref 29.

Detection of low amounts of ricin was particularly problematic with the DHLA-coated QDs due to high background binding of the QDs to the assay plate. We attribute this effect to both the charged ligand and the pH utilized, which contributed to the larger error in this K_d calculation. For this reason, as well as for the limited pH-solubility issues, DHLA may not be an ideal surface ligand for such QD based immunosensors. The CL4 QDs

dx.doi.org/10.1021/bc300644p | Bioconjugate Chem. 2013, 24, 269−281

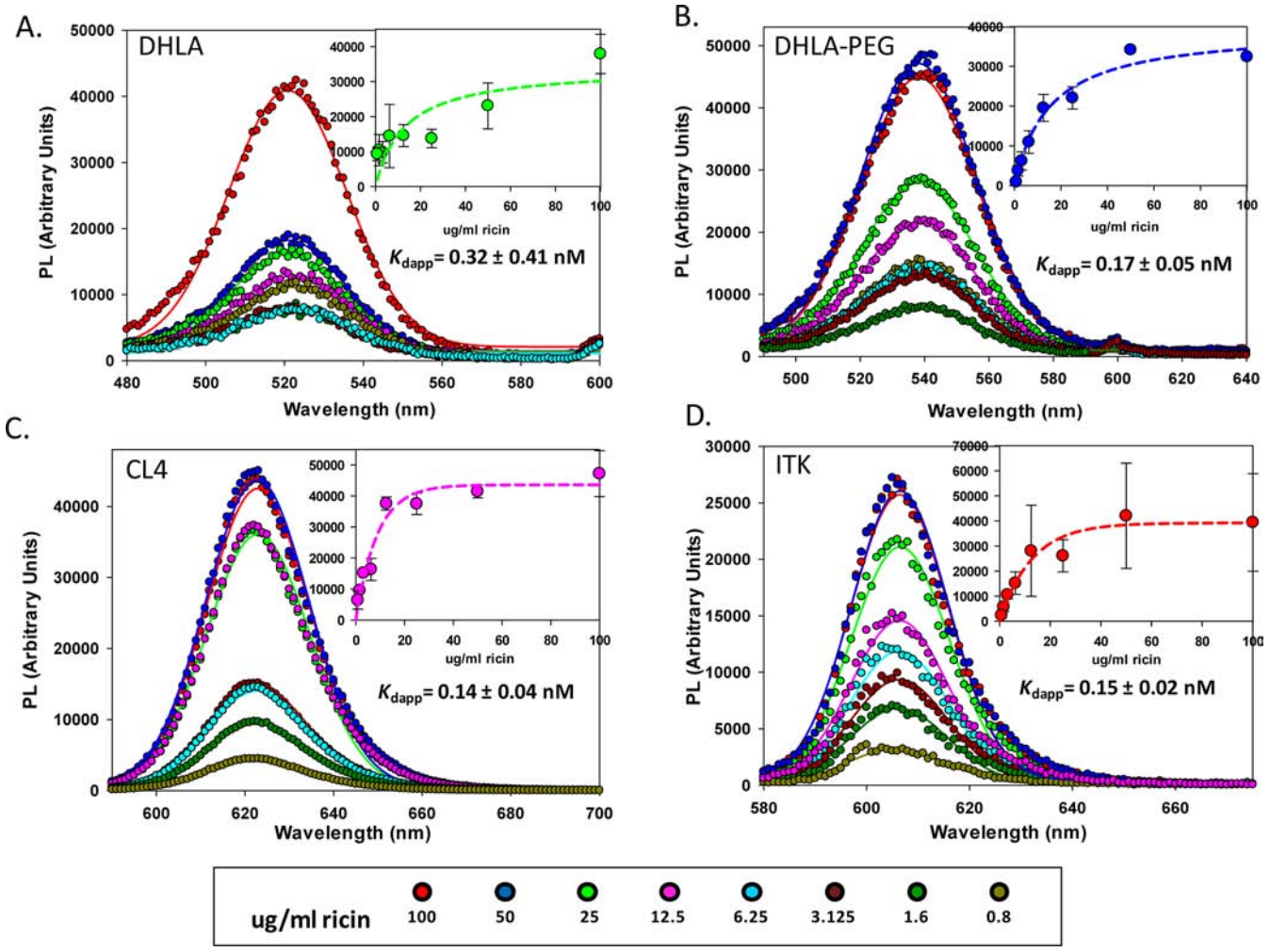

Figure 4. Representative titration of each of the QD materials assembled with C8-2OQQ-His_6 sdAb against the indicated increasing concentrations of ricin: (A) DHLA-QDs, (B) DHLA-PEG-QDs, (C) CL4-QDs, (D) carboxylated ITK QDs. Insets show binding curves and estimated K_d values.

Table 3. Apparent Sensing Parameters Estimated in This Study[a]

surface ligand	K_{dapp} (nM)	limit of detection (ng/mL) LOD_{app}	dynamic sensing range (ng/mL) DSR_{app}
DHLA	0.32 ± 0.41	8700	1470−119 000
DHLA-PEG	0.17 ± 0.05	2450	1700−137 000
ITK	0.15 ± 0.02	210	1200−99 000
CL4	0.14 ± 0.04	50	850−68 500

[a]LOD was estimated as 3× the standard deviation of the maximum PL with 0 μg/mL ricin. Dynamic sensing range was estimated using 10−90% of the maximum PL for each QD in a ricin titration assay. LOD and sensing range values are rounded up to the nearest 10 or 100 value.

appear to perform the best, supporting a positive role for smaller, more compact, and pH-flexible surface ligands during His_n-driven metal affinity coordination.[21] Interestingly, the ITK based biosensor performed similarly to the DHLA-PEG QD sensors, indicating that there is little difference in antigen recognition whether the antibody binds directly to the QD surface or the carboxyl ends of the surface ligands. The latter result in essence provides strong evidence of oriented binding to the QDs with the sdAb binding site remaining available. Clearly, all three DHLA-PEG, CL4, and ITK QD types can successfully be used as central fluorescent probes and nanoassembly platforms for sdAb application in immunoassay formats.

Simulation of QD and Modified sdAb Structures. We have frequently modeled the interactions of proteins and peptides with QDs in order to gain insight into the final bioconjugate structure/function relationship.[14,18,39,48] A similar approach was undertaken here in order to understand the differences between the three primary constructs, namely, the C8-His_6, C8-1BYZ-His_6, and C8-2OQQ-His_6 sdAb proteins. The protein structures were simulated as described in the Methods and Supporting Information and are presented in Figure 5 in comparison to a QD surface functionalized with the DHLA-PEG ligand. In searching the PDB for a structure related to the anti-ricin C8, many of the sdAbs found displayed strong overlapping homology and so this portion of the structure should be extremely conserved and invariant. In contrast, the portion of the sequence between the central sdAb globular protein and either the His_6-tail or helical linker insertion sites was found to have almost no reported structure indicating that this segment was quite malleable or random and did not assume any fixed structure, especially during crystallography. This portion is highlighted in the 1BYZ structure in Figure 5.

The final conformations of the helical linkers and His_6-tail relative to the central protein portion in the three constructs may never be fully determined (due to the above-mentioned lack of structure), and it is important to note that the linkers have a large degree of freedom and can assume almost any conformation

dx.doi.org/10.1021/bc300644p | Bioconjugate Chem. 2013, 24, 269−281

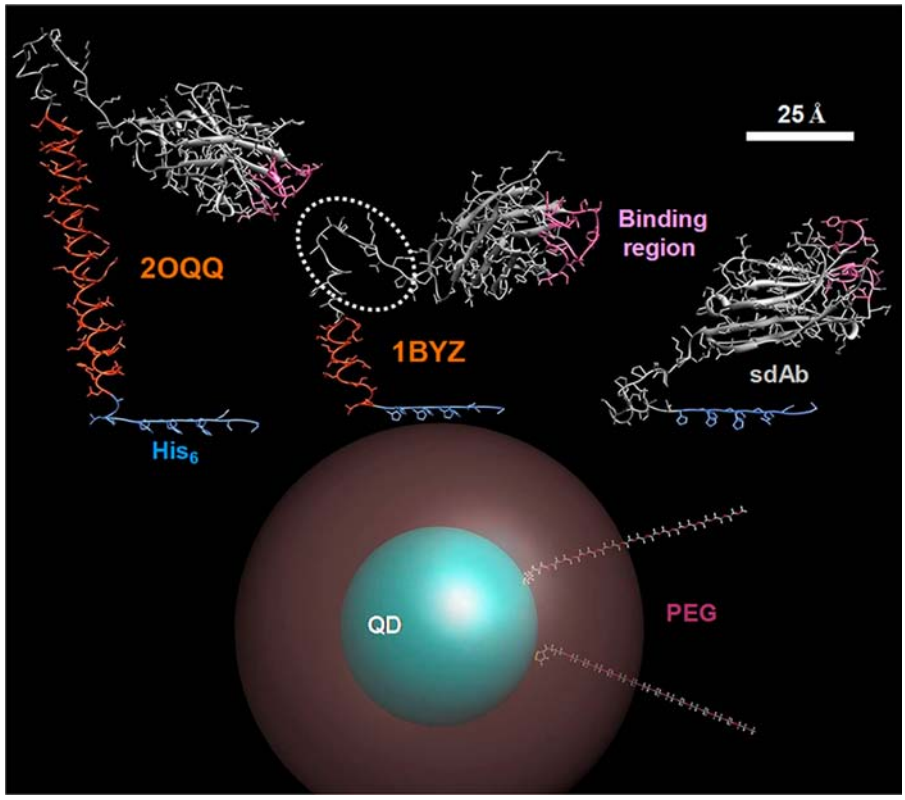

Figure 5. Schematic illustration of a PEGylated QD and structural models of the C8-His_6 sdAb (right), C8-1BYZ-His_6 sdAb (middle), and the C8-2OQQ-His_6 sdAb (left). The QD with a nominal diameter of 56 Å is shown in aqua surrounded by a PEG shell (maroon). The structure of two DHLA-PEG-OMe molecules is shown in a fully extended conformation, while the PEG shell reflects the more probable, energy-minimized conformation with an extension of ~28.5 Å as determined experimentally.[21] For the sdAb constructs, the main globular protein is shown in gray with the binding region highlighted in pink. The 2OQQ and 1BYZ linkers are shown in orange and the terminal His_6 on each is highlighted in blue. The central 1BYZ construct also has a dashed oval highlighting the highly flexible/hinge portion of the structure. Note that this simulation is to scale.

ranging from folded onto the central protein to extending directly away from it. However, the simulations in Figure 5 do serve to reflect the reasons for some of the QD interactions and subsequent findings described here. It is probable that the His_6-tail on the C8-His_6 sdAb is closely associated with the central protein structure and does not extend out enough to overcome steric constraints imposed by the QD PEG layer. This simulation, in essence, serves to confirm our initial supposition that steric hindrance prevented the metal affinity coordination of this protein to the surface of PEGylated QDs. The addition of the smaller 1BYZ linker to the construct does provide a slight improvement—but this is still not significant (see Figure 3A). However, the length and especially the rigidity of the 2OQQ helix are significant enough to allow the His_6-tail to penetrate the PEG layer. It may be able to accomplish this regardless of whether the helix is adjacent to or folding over the central protein portion. This ability should also hold true for the polymer-functionalized ITK QDs, and the improvements here may again reflect the ability of this long linker to penetrate into the surrounding ligand and access "buried" attachment sites. Overall, the simulation also suggests that a relatively long and highly persistent helix placed between a terminal His_6-tail and the central globular portion of many proteins may help to make the tail more available for metal-affinity coordination to QD surfaces.

■ DISCUSSION AND CONCLUSIONS

The binding of proteins to QD surfaces is necessary for the development of many kinds of QD-based probes and biosensors. The general inability of globular proteins to self-assemble directly to the surface of DHLA-PEG coated QDs has been problematic, and its resolution is an important advancement to allow further development of QD-based biosensors. One approach to addressing this has been to synthesize more complex QD ligands that display terminal NTA groups, and indeed, there are several such examples in the literature.[1,49] In addition to the added synthetic steps required to prepare these ligands, this generally increases both the size of the final ligand and the hydrodynamic size of the final conjugate itself. Here, we evaluate how appending and extending terminally expressed polyhistidine linkers can allow globular proteins to self-assemble to QDs surface-capped with a variety of different chemical compositions. We use the C8 anti-ricin sdAb and an immunoassay format as a mechanism to confirm assembly to the QDs and as a way to further verify that the proteins are indeed still functional.

The issues surrounding His-driven assembly of proteins to QDs coated with different ligands have been previously investigated by Dennis et al. who systematically analyzed the interactions of QDs displaying various coatings with a His_6-appended mCherry fluorescent protein.[24] They found that decreased ligand size, or interaction with ligand ends, such as the carboxyl ends of ITK QDs greatly improved His-tagged protein binding ability. Here, we show that we can provide binding to globular proteins and even further improve existing binding interactions by engineering long helical linkers between the protein coding sequence and the terminal His_6. Not surprisingly, the longest helical linker provided for better assembly overall. Additionally, binding to QDs decorated with compact ligand coatings like DHLA and CL4 benefitted from the presence of linkers. We hypothesize that these linkers increase

dx.doi.org/10.1021/bc300644p | Bioconjugate Chem. 2013, 24, 269−281

the ability of the His_6 tag to penetrate the surface ligand layer and bind the QD surface in a cooperative manner. It is also possible that the neighboring terminal carboxyl groups present on the CL4 ligand (Scheme 1) could interact in a chelating manner to coordinate the His_6 groups; however, it is important to note that the assay media for these QD conjugates was not supplemented with any divalent cations, which could potentially enhance this effect. Increasing the number of appended $(His)_n$ tags did not provide any assembly improvement somewhat reflecting the kinetics measured for increasing $(His)_n$ repeat number on direct QD assembly; no significant improvements of binding affinity to QDs have been noted beyond the $n = 6$ here, although this point must be qualified by the fact that each $(His)_6$ in the $(His_6)_3$ constructs is separated by 6 residues which could be detrimental for cooperative assembly.[19] This lack of improvement is somewhat in contrast to other reports where increasing the number and reorienting the $(His)_6$ tags into a dendritic-type wedge arrangement appeared to increase affinity.[50,51]

As the metal-affinity coordination of $(His)_n$ to the QDs is quite stable above pH 5 or so, use of different pH buffers and net protein charge (Table 1) appeared to have no discernible impact on initial assembly or stability of the bioconjugate, except for the DHLA-based results.[19] Interestingly, QDs displaying ligands with peptide attachment points displaced away from the QD surface, such as ITK QDs, also showed improved binding with the linkers. We hypothesize that the increased length and flexibility of the linker allows for better penetration into the polymer layer and access to carboxyl groups not available to the surface. This leads to better binding with the QD and ultimately better sensor performance. The similar K_d values strongly suggest that attachment to the different QD surfaces does not allosterically alter the protein binding properties. As the terminal $(His)_n$ is located at the opposite end of the sdAb from the antigen binding site, the proteins are most likely assembled to all the QDs in an oriented manner with the binding sites clearly available.

There have been a number of newly developed chemoselective chemistries[1,16,52−54] that do ameliorate many of the functional issues associated when using EDC or biotin−avidin chemistry for QD-biolabeling. Despite the improvements, these approaches still have liabilities especially in the case of protein attachment, as they still often target the ubiquitous amines that are present on the proteins. This point helps highlight the fact that there is still room for a variety of different QD-bioconjugation chemistries and that having access to different choices can help improve the function of particular assemblies.

There are many inherent benefits of His_n-based assembly to QDs which may cumulatively help drive the popularity of this bioconjugation approach with linker-modified proteins. These include its general applicability to many types of QD preparations (including commercial materials) as exemplified here, the long-term stability and high affinity of the interaction, the limited number of preparation steps required (essentially mixing), and providing conjugates with control over both protein valence and the display orientation. To facilitate attaching linkers to any expressed protein, plasmids can be quickly configured that provide both the linker and a terminal His_n-tag along with a centrally located cloning site. The His_n-tag would serve two roles here, providing for both initial purification of the recombinant protein and later QD assembly. Beyond QDs, these same proteins should be able to bind to almost any surface or other nanoparticle material that displays the appropriate divalent metal cation or metal cation chelate such as an NTA group. More investigation is still needed to better understand how these linkers function and especially to determine if they show similar binding enhancements with other proteins, or if a wide range of linker constructs are needed for optimal use with many different protein structures/sizes. It is also probable that further optimization of surface ligand design could also contribute to improved assembly and binding/targeting kinetics for any attached protein. Overall, combining compact QD surface ligands and proper linker/protein engineering should allow the terminal His_6-tag accessibility for the binding of almost all globular proteins to QD surfaces. Optimization of this process will open the door for a myriad of QD-protein biosensors that were previously unattainable.

■ ASSOCIATED CONTENT

Supporting Information

This includes additional experimental results and details of the structural simulation. This material is available free of charge via the Internet at http://pubs.acs.org.

■ AUTHOR INFORMATION

Corresponding Author

*E-mail: Igor.medintz@nrl.navy.mil.

Notes

The authors declare no competing financial interest.

■ ACKNOWLEDGMENTS

The authors thank D. Prasuhn for technical assistance with peptide preparation and acknowledge the NRL NSI, DARPA, and DTRA JSTO MIPR # B112582M.

■ REFERENCES

(1) Algar, W. R., Susumu, K., Delehanty, J. B., and Medintz, I. L. (2011) Quantum dots in bioanalysis: Crossing the valley of death. *Anal. Chem. 83*, 8826−8837.

(2) Alivisatos, A. P., Gu, W., and Larabell, C. A. (2005) Quantum dots as cellular probes. *Ann. Rev. Biomed. Eng. 7*, 55−76.

(3) Michalet, X., Pinaud, F. F., Bentolila, L. A., Tsay, J. M., Doose, S., Li, J. J., Sundaresan, G., Wu, A. M., Gambhir, S. S., and Weiss, S. (2005) Quantum dots for live cells, in vivo imaging, and diagnostics. *Science 307*, 538−544.

(4) Rosenthal, S. J., Chang, J. C., Kovtun, O., McBride, J. R., and Tomlinson, I. D. (2011) Biocompatible quantum dots for biological applications. *Chem. Biol. 18*, 10−24.

(5) Ho, Y. P., and Leong, K. W. (2010) Quantum dot-based theranostics. *Nanoscale 2*, 60−68.

(6) Zrazhevskiy, P., Sena, M., and Gao, X. (2010) Designing multifunctional quantum dots for bioimaging, detection, and drug delivery. *Chem. Soc. Rev. 39*, 4326−4354.

(7) Medintz, I. L., Mattoussi, H., and Clapp, A. R. (2008) Potential clinical applications of quantum dots. *Int. J. Nanomed. 3*, 151−167.

(8) Delehanty, J. B., Boeneman, K., Bradburne, C. E., Robertson, K., and Medintz, I. L. (2009) Quantum dots: a powerful tool for understanding the intricacies of nanoparticle-mediated drug delivery. *Expert Opin. Drug Delivery 6*, 1091−1112.

(9) Algar, W. R., and Krull, U. J. (2010) New opportunities in multiplexed optical bioanalyses using quantum dots and donor-acceptor interactions. *Anal. Bioanal. Chem. 398*, 2439−2449.

(10) Medintz, I. L., and Mattoussi, H. (2009) Quantum dot-based resonance energy transfer and its growing application in biology. *Phys. Chem. Chem. Phys. 11*, 17−45.

(11) Barroso, M. M. (2011) Quantum dots in cell biology. *J. Histochem. Cytochem. 59*, 237−251.

(12) Byers, R. J., and Hitchman, E. R. (2011) Quantum dots brighten biological imaging. *Prog. Histochem. Cytochem. 45*, 201−237.

(13) Xing, Y., Xia, Z. Y., and Rao, J. H. (2009) Semiconductor quantum dots for biosensing and in vivo imaging. *IEEE Trans. Nanobiosci. 8*, 4−12.
(14) Goldman, E. R., Medintz, I. L., Whitley, J. L., Hayhurst, A., Clapp, A. R., Uyeda, H. T., Deschamps, J. R., Lassman, M. E., and Mattoussi, H. (2005) A hybrid quantum dot-antibody fragment fluorescence resonance energy transfer-based TNT sensor. *J. Am. Chem. Soc. 127*, 6744−6751.
(15) Medintz, I. L. (2006) Universal tools for biomolecular attachment to surfaces. *Nat. Mater. 5*, 842−842.
(16) Algar, W. R., Prasuhn, D. E., Stewart, M. H., Jennings, T. L., Blanco-Canosa, J. B., Dawson, P. E., and Medintz, I. L. (2011) The controlled display of biomolecules on nanoparticles: A challenge suited to bioorthogonal chemistry. *Bioconjugate Chem. 22*, 825−858.
(17) Hermanson, G. T. *Bioconjugate Techniques*, 2nd ed. (2008) Academic Press, San Diego.
(18) Boeneman, K., Deschamps, J. R., Buckhout-White, S., Prasuhn, D. E., Blanco-Canosa, J. B., Dawson, P. E., Stewart, M. H., Susumu, K., Goldman, E. R., Ancona, M., and Medintz, I. L. (2010) Quantum dot DNA bioconjugates: Attachment chemistry strongly influences the resulting composite architecture. *ACS Nano 4*, 7253−7266.
(19) Sapsford, K. E., Pons, T., Medintz, I. L., Higashiya, S., Brunel, F. M., Dawson, P. E., and Mattoussi, H. (2007) Kinetics of metal-affinity driven self-assembly between proteins or peptides and CdSe-ZnS quantum dots. *J. Phys. Chem. C 111*, 11528−11538.
(20) Liu, W., Howarth, M., Greytak, A. B., Zheng, Y., Nocera, D. G., Ting, A. Y., and Bawendi, M. G. (2008) Compact biocompatible quantum dots functionalized for cellular imaging. *J. Am. Chem. Soc. 130*, 1274−1284.
(21) Susumu, K., Oh, E., Delehanty, J. B., Blanco-Canosa, J. B., Johnson, B. J., Jain, V., Hervey, W. J., Algar, W. R., Boeneman, K., Dawson, P. E., and Medintz, I. L. (2011) Multifunctional compact zwitterionic ligands for preparing robust biocompatible semiconductor quantum dots and gold nanoparticles. *J. Am. Chem. Soc. 133*, 9480−9496.
(22) Zhang, Y., So, M. K., Loening, A. M., Yao, H. Q., Gambhir, S. S., and Rao, J. H. (2006) HaloTag protein-mediated site-specific conjugation of bioluminescent proteins to quantum dots. *Angew. Chem., Int. Ed. 45*, 4936−4940.
(23) Yao, H., Zhang, Y., Xiao, F., Xia, Z., and Rao, J. (2007) Quantum dot/bioluminescence resonance energy transfer based highly sensitive detection of proteases. *Angew. Chem., Int. Ed. 46*, 4346−4349.
(24) Dennis, A. M., Sotto, D. C., Mei, B. C., Medintz, I. L., Mattoussi, H., and Bao, G. (2010) Surface ligand effects on metal-affinity coordination to quantum dots: Implications for nanoprobe self-assembly. *Bioconjugate Chem. 21*, 1160−1170.
(25) Lu, H., Schops, O., Woggon, U., and Niemeyer, C. M. (2008) Self-assembled donor comprising quantum dots and fluorescent proteins for long-range fluorescence resonance energy transfer. *J. Am. Chem. Soc. 130*, 4815−4827.
(26) Mei, B. C., Susumu, K., Medintz, I. L., Delehanty, J. B., Mountziaris, T. J., and Mattoussi, H. (2008) Modular poly(ethylene glycol) ligands for biocompatible semiconductor and gold nanocrystals with extended pH and ionic stability. *J. Mater. Chem. 18*, 4949−4958.
(27) Oh, J. K. (2010) Surface modification of colloidal CdX-based quantum dots for biomedical applications. *J. Mater. Chem. 20*, 8433−8445.
(28) Uyeda, H. T., Medintz, I. L., Jaiswal, J. K., Simon, S. M., and Mattoussi, H. (2005) Synthesis of compact multidentate ligands to prepare stable hydrophilic quantum dot fluorophores. *J. Am. Chem. Soc. 127*, 3870−3878.
(29) Anderson, G. P., Liu, J. L., Hale, M. L., Bernstein, R. D., Moore, M., Swain, M. D., and Goldman, E. R. (2008) Development of antiricin single domain antibodies toward detection and therapeutic reagents. *Anal. Chem. 80*, 9604−9611.
(30) Sapsford, K. E., Farrell, D., Sun, S., Rasooly, A., Mattoussi, H., and Medintz, I. L. (2008) Monitoring of enzymatic proteolysis on a electroluminescent-CCD microchip platform using quantum dot-peptide substrates. *Sens. Actuators, B 139*, 13−21.
(31) Lakowicz, J. R. (2006) *Principles of Fluorescence Spectroscopy*, 3rd ed., Springer, New York.
(32) Clapp, A. R., Medintz, I. L., Mauro, J. M., Fisher, B. R., Bawendi, M. G., and Mattoussi, H. (2004) Fluorescence resonance energy transfer between quantum dot donors and dye-labeled protein acceptors. *J. Am. Chem. Soc. 126*, 301−310.
(33) Pons, T., Medintz, I. L., Wang, X., English, D. S., and Mattoussi, H. (2006) Solution-phase single quantum dot fluorescence resonance energy transfer. *J. Am. Chem. Soc. 128*, 15324−15331.
(34) Boeneman, K., Delehanty, J. B., Susumu, K., Stewart, M. H., and Medintz, I. L. (2010) Intracellular bioconjugation of targeted proteins with semiconductor quantum dots. *J. Am. Chem. Soc. 132*, 5975−5977.
(35) Pettersen, E. F., Goddard, T. D., Huang, C. C., Couch, G. S., Greenblatt, D. M., Meng, E. C., and Ferrin, T. E. (2004) UCSF Chimera–a visualization system for exploratory research and analysis. *J. Comput. Chem. 25*, 1605−1612.
(36) Prive, G. G., Anderson, D. H., Wesson, L., Cascio, D., and Eisenberg, D. (1999) Packed protein bilayers in the 0.90 A resolution structure of a designed alpha helical bundle. *Protein Sci. 8*, 1400−9.
(37) Yoon, M. K., Kim, H. M., Choi, G., Lee, J.-O., and Choi, B.-S. (2007) Structural basis for the conformational integrity of the Arabidopsis thaliana HY5 leucine zipper homodimer. *J. Biol. Chem. 282*, 12989−13002.
(38) Kuliopulos, A., and Walsh, C. T. (1994) Production, purification, and cleavage of tandem repeats of recombinant peptides. *J. Am. Chem. Soc. 116*, 4599−4607.
(39) Boeneman, K., Prasuhn, D. E., Blanco-Canosa, J. B., Dawson, P. E., Melinger, J. S., Ancona, M., Stewart, M. H., Susumu, K., Huston, A., and Medintz, I. L. (2010) Self-assembled quantum dot-sensitized multivalent DNA photonic wires. *J. Am. Chem. Soc. 132*, 18177−18190.
(40) de Marco, A. (2011) Biotechnological applications of recombinant single-domain antibody fragments. *Microbial Cell Factories 10*, 44.
(41) Anderson, G. P., Bernstein, R. D., Swain, M. D., Zabetakis, D., and Goldman, E. R. (2010) Binding kinetics of antiricin single domain antibodies and improved detection using a B chain specific binder. *Anal. Chem. 82*, 7202−7207.
(42) Walper, S. A., Anderson, G. P., Lee, P. A. B., Glaven, R. H., Liu, J. L., Bernstein, R. D., Zabetakis, D., Johnson, L., Czarnecki, J. M., and Goldman, E. R. (2012) Rugged single domain antibody detection elements for Bacillus anthracis spores and vegetative dells. *Plos One 7*, 10.
(43) Hochuli, E., Bannwarth, W., Dobeli, H., Gentz, R., and Stuber, D. (1988) Genetic approach to facilitate purification of recombinant proteins with a novel metal chelate adsorbent. *Biotechnology 6*, 1321−1325.
(44) Herman, C., Thevenet, D., Bouloc, P., Walker, G. C., and D'Ari, R. (1998) Degradation of carboxy-terminal-tagged cytoplasmic proteins by the Escherichia coli protease HflB (FtsH). *Genes Dev. 12*, 1348−1355.
(45) Prasuhn, D. E., Deschamps, J. R., Susumu, K., Stewart, M. H., Boeneman, K., Blanco-Canosa, J. B., Dawson, P. E., and Medintz, I. L. (2010) Polyvalent display and packing of peptides and proteins on semiconductor quantum dots: predicted versus experimental results. *Small 6*, 555−564.
(46) Pons, T., Uyeda, H. T., Medintz, I. L., and Mattoussi, H. (2006) Hydrodynamic dimensions, electrophoretic mobility and stability of hydrophilic quantum dots. *J. Phys. Chem. B 110*, 20308−20316.
(47) Medintz, I. L., Goldman, E. R., Lassman, M. E., and Mauro, J. M. (2003) A fluorescence resonance energy transfer sensor based on maltose binding protein. *Bioconjugate Chem. 14*, 909−918.
(48) Medintz, I. L., Konnert, J. H., Clapp, A. R., Stanish, I., Twigg, M. E., Mattoussi, H., Mauro, J. M., and Deschamps, J., R. (2004) A fluorescence resonance energy transfer derived structure of a quantum dot-protein bioconjugate nanoassembly. *Proc. Natl. Acad. Sci. U.S.A 101*, 9612−9617.
(49) Susumu, K., Medintz, I. L., Delehanty, J. B., Boeneman, K., and Mattoussi, H. (2010) Modification of poly(ethylene glycol)-capped

quantum dots with nickel nitrilotriacetic acid and self-assembly with histidine-tagged proteins. *J. Phys. Chem. C 114*, 13526−13531.
(50) Wang, J. H., Jiang, P. J., Han, Z. Y., Qiu, L., Wang, C. L., Zheng, B., and Xia, J. (2012) Fast self-assembly kinetics of quantum dots and a dendrimeric peptide ligand. *Langmuir 28*, 7962−7966.
(51) Wang, J. H., and Xia, J. (2011) Preferential binding of a novel polyhistidine peptide dendrimer ligand on quantum dots probed by capillary electrophoresis. *Anal. Chem. 83*, 6323−6329.
(52) Jennings, T. L., Becker-Catania, S. G., Triulzi, R. C., Tao, G., Scott, B., Sapsford, K. E., Spindel, S., Oh, E., Jain, V., Delehanty, J. B., Prasuhn, D. E., Boeneman, K., Algar, W. R., and Medintz, I. L. (2011) Reactive semiconductor nanocrystals for chemoselective bio-labeling and multiplexed analysis. *ACS Nano 5*, 5579−5593.
(53) Hildebrandt, N. (2011) Biofunctional quantum dots: Controlled conjugation for multi-plexed biosensors. *ACS Nano 5*, 5286−5290.
(54) Blanco-Canosa, J. B., Medintz, I. L., Farrell, D., Mattoussi, H., and Dawson, P. E. (2010) Rapid covalent ligation of fluorescent peptides to water solubilized quantum dots. *J. Am. Chem. Soc. 132*, 10027−10033.